Finite element formulation of smart piezoelectric composite plates coupled with acoustic fluid

Walid Larbi, Jean-François Deü, Roger Ohayon

Finite element formulation of smart piezoelectric composite plates coupled with acoustic fluid

W. Larbi, J.-F. Deü *, R. Ohayon

Structural Mechanics and Coupled Systems Laboratory, Conservatoire National des Arts et Métiers, 292 rue Saint-Martin, 75141 Paris Cedex 03, France

In the context of noise and vibration reduction by passive piezoelectric devices, this work presents the theoretical formulation and the finite element (FE) implementation of vibroacoustic problems with pie-zoelectric composite structures connected to electric shunt circuits. The originalities of this work concern (i) the formulation of the electro-mechanical-acoustic coupled system, (ii) the implementation of an accurate and inexpensive laminated composite plate FE with embedded piezoelectric layers connected to resonant shunt circuits, and (iii) the development of an efficient fluid–structure interface element. Var-ious results are presented in order to validate and illustrate the performance of the proposed fully cou-pled numerical approach.

1. Introduction

For noise and vibration reduction, various approaches can be employed depending on the frequency range to attenuate. Generally, active or passive piezoelectric techniques are effective in the low frequency range, while dissipative materials, such as viscoelastic treatments or porous insulation, are efficient for higher frequency domain. This work presents the theoretical formulation and the finite element (FE) implementation of multilayer piezoelectric plates coupled with acoustic fluid and connected to resonant shunt circuits.

The modeling and analysis of laminated piezoelectric structures is an active area of research as attested by the large number of papers published in the literature (see, e.g. [9,7] for beams and [8,14,2,11] for plates). Careful analysis of the corresponding articles indicates that approximate theories mainly differ by the simplifying a priori assumptions concerning the piezoelectric effect representation, the directions of the electric field and the through-thickness distributions of the mechanical displacements and electric potential. Hence, regarding these criteria, the various reported theories can be separated into uncoupled and coupled ones, depending on the presence or not of electric fundamental variables [1]. Available models can also be classified into global or equivalent single-layer models, and discrete layer or layerwise ones, depending on the through-thickness variations of the mechanical and electric fields. Even if the development of multilayer piezoelectric plate theories has reached a relative maturity, computational modeling of structural–acoustic problems with piezoelectric elements is less studied and represents an expanding research field. For noise and vibration reduction applications in the low frequency range, active-control using piezoelectric devices is an affective approach. In this context, let us mention [16,19] where active controller designs are developed to reduce interior cabin noise levels and [27,25] where active/passive constrained layer damping treatments are proposed to control sound radiation from a vibrating thin structure into an acoustic cavity. Structural–acoustic vibration reduction using passive (shunted) or semi-passive (switched) piezoelectric techniques is also proposed in the literature [12,18]. For the modeling and design of such fluid–structure problems, FE method is generally used [22,24,5]. Another approach consists in combining the FE method for the dynamic analysis of the smart structure and the boundary element method to evaluate the acoustic response of the enclosed fluid. In such a case, the steady-state response of acoustic cavities bounded by piezoelectric composite shell structures is proposed in [15] and an active–passive control technique, based an output feedback optimal controller design, is developed in [10].

In the first part of this paper, a non-symmetric finite element formulation of the coupled system is derived from a variational principle involving structural displacement, electrical voltage of piezoelectric patches, and acoustic pressure in the fluid cavity. This formulation, with only one couple of electric variables per patch, is well adapted to practical applications since realistic electrical boundary conditions, such that equipotential electrodes and prescribed global electric charges, naturally appear. The global charge/voltage variables are intrinsically adapted to include any external electrical circuit into the electromechanical problem and to simulate the effect of resistive or resonant shunt damping techniques.

* Corresponding author.
E-mail address: jean-francois.deu@cnam.fr (J.-F. Deü).

The second part of this work is devoted to the development of (i) an efficient finite element piezoelectric laminated plate, and (ii) an appropriate interface element to ensure the interaction between fluid and structure. The composite plate model, with piezoelectric layers polarized along the thickness, combines an equivalent single-layer approach for the mechanical behavior with a layerwise representation of the electric potential in the thickness direction. A four nodes finite element layered plate, with five degrees-of-freedom (dof) per node, is then developed. The in-plane displacements are discretized by conforming bi-linear Lagrange shape functions, while the transverse displacement and rotations are discretized by nonconforming cubic Hermite shape functions. This choice is proved to be efficient compared to other FE models and well adapted to structural–acoustic applications. For the electric behavior, only one degree-of-freedom per piezoelectric layer is used allowing to including any shunt circuit connected to piezoelectric patches in order to simulate the vibration attenuation.

Finally, some numerical examples are presented in order to validate and demonstrate the effectiveness of the proposed fluid-piezoelectric-structure finite element approach.

2. Variational formulation of internal structural–acoustic coupled problems with piezoelectric shunt systems

We briefly recall in this section the variational formulation of internal structural–acoustic coupled problems with shunted piezoelectric patches connected to the vibrating structure. This formulation is written in terms of structural mechanical displacement u_i, electric potential difference between the upper and the lower electrode of each patch $V^{(p)} = \psi_+^{(p)} - \psi_-^{(p)}$ and fluid pressure p (for more details, we refer the reader to [17,5]).

An elastic structure occupying the domain Ω_E is equipped with P piezoelectric patches and completely filled with an internal inviscid linear acoustic fluid occupying the domain Ω_F (Fig. 1). Each piezoelectric patch has the shape of a thin plate with its upper and lower surfaces covered with a very thin layer electrode. The pth patch, $p \in \{1,\dots,P\}$, occupies a domain $\Omega^{(p)}$ such that (Ω_E, $\Omega^{(1)},\dots,\Omega^{(P)}$) is a partition of the all structure domain Ω_S. In order to reduce the vibration amplitudes of the coupled problem, a resonant shunt circuit with a resistor $R^{(p)}$ and inductor $L^{(p)}$ in series is connected to each patch [13,18].

We denote by Σ the fluid–structure interface and by n_i^S and n_i^F the unit normal external to Ω_S and Ω_F, respectively. The structure is clamped on a part Γ_u and subjected to a given surface force density F_i^d on the complementary part Γ_σ of its external boundary and to a pressure field p due to the presence of the fluid on its internal boundary Σ.

The linearized deformation tensor is $\varepsilon_{ij} = \frac{1}{2}(u_{i,j} + u_{j,i})$ and the stress tensor is denoted by σ_{ij}. Moreover, D_i denotes the electric displacement and E_i the electric field such that $E_i = -\psi_{,i}$. The linear piezoelectric constitutive equations write:

$$\sigma_{ij} = c_{ijkl}\varepsilon_{kl} - e_{kij}E_k \tag{1}$$

$$D_i = e_{ikl}\varepsilon_{kl} + \epsilon_{ik}E_k \tag{2}$$

where c_{ijkl} denotes the elastic moduli at constant electric field, e_{kij} the piezoelectric constants and ϵ_{ik} the dielectric permittivities at constant strain.

For each piezoelectric patch, a set of hypotheses, which can be applied to a wide spectrum of practical applications, are formulated:

- The piezoelectric patches are thin, with a constant thickness, denoted $h^{(p)}$ for the pth patch;
- The thickness of the electrodes is much smaller than $h^{(p)}$ and is thus neglected;
- The piezoelectric patches are polarized in their transverse direction (i.e. the direction normal to the electrodes).

Under those assumptions, the electric field vector, of components $E_k^{(p)}$, can be considered normal to the electrodes and uniform in the piezoelectric patch [28], so that for all $p \in \{1,\dots,P\}$:

$$E_k^{(p)} = -\frac{V^{(p)}}{h^{(p)}} n_k \quad \text{in} \quad \Omega^{(p)} \tag{3}$$

where $V^{(p)}$ is constant over $\Omega^{(p)}$ and n_k is the kth component of the normal unit vector to the surface of the electrodes.

By considering successively each of the $P+2$ subdomains Ω_F, Ω_E and ($\Omega^{(1)},\dots,\Omega^{(P)}$), the variational formulation of the fluid/structure/piezoelectric-patches coupled system can be written in terms of the structural mechanical displacement u_i, the electric potential difference $V^{(p)}$ constant in each piezoelectric patch, and the fluid pressure p:

- Mechanical equation:

$$\int_{\Omega_S} c_{ijkl}\varepsilon_{kl}\delta\varepsilon_{ij}\,\mathrm{d}v + \sum_{p=1}^{P}\frac{V^{(p)}}{h^{(p)}}\int_{\Omega^{(p)}} e_{kij}n_k\delta\varepsilon_{ij}\,\mathrm{d}v + \int_{\Omega_S}\rho_S\frac{\partial^2 u_i}{\partial t^2}\,\delta u_i\,\mathrm{d}v - \int_{\Sigma} p\,n_i^F\,\delta u_i\,\mathrm{d}s = \int_{\Gamma_\sigma} F_i^d\,\delta u_i\,\mathrm{d}s \quad \forall \delta u_i \in C_u^* \tag{4}$$

where ρ_S is the mass density of the structure and where the admissible space C_u^* is defined by $C_u^* = \{u_i \in C_u \mid u_i = 0 \text{ on } \Gamma_u\}$. C_u being the admissible space of regular functions u in Ω_s.

- Electrical equation:

$$\sum_{p=1}^{P}\delta V^{(p)}C^{(p)}V^{(p)} - \sum_{p=1}^{P}\frac{\delta V^{(p)}}{h^{(p)}}\int_{\Omega^{(p)}} e_{ikl}\varepsilon_{kl}n_i\,\mathrm{d}v = \sum_{p=1}^{P}\delta V^{(p)}Q^{(p)} \quad \forall \delta V^{(p)} \in \mathbb{R} \tag{5}$$

where $C^{(p)} = \epsilon_{33}S^{(p)}/h^{(p)}$ defines the capacitance of the blocked pth piezoelectric patch ($S^{(p)}$ being the area of the patch and $\epsilon_{33} = \epsilon_{ik}n_i n_k$ the piezoelectric material permittivity in the direction normal to the electrodes) and $Q^{(p)}$ is the global charge in one of the electrodes (see [28]).

- Acoustic equation:

$$\frac{1}{\rho_F}\int_{\Omega_F} p_{,i}\,\delta p_{,i}\,\mathrm{d}v + \frac{1}{\rho_F c_F^2}\int_{\Omega_F}\frac{\partial^2 p}{\partial t^2}\,\delta p\,\mathrm{d}v + \int_{\Sigma}\frac{\partial^2 u_i}{\partial t^2}\,n_i^F\,\delta p\,\mathrm{d}s = 0 \quad \forall \delta p \in C_p \tag{6}$$

where c_F is the constant speed of sound in the fluid, ρ_F the mass density of the fluid and C_p is the admissible space of regular functions p defined in Ω_F (see [22] for more details).

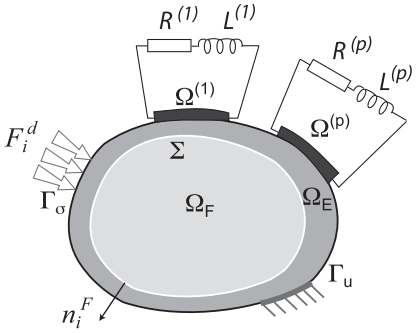

Fig. 1. Vibrating structure coupled with acoustic cavity and connected to *RL* shunt circuits.

After discretizing the variational formulation by the finite element method and using the following additional relation between electrical potential differences and electric charges due to the shunt circuits:

$$\mathbf{L}\ddot{\mathbf{Q}} + \mathbf{R}\dot{\mathbf{Q}} + \mathbf{V} = \mathbf{0} \tag{7}$$

we find the following matrix system:

$$\begin{bmatrix} \mathbf{M}_u & \mathbf{0} & \mathbf{0} \\ \mathbf{0} & \mathbf{L} & \mathbf{0} \\ \mathbf{C}_{up}^T & \mathbf{0} & \mathbf{M}_p \end{bmatrix} \begin{bmatrix} \ddot{\mathbf{U}} \\ \ddot{\mathbf{Q}} \\ \ddot{\mathbf{P}} \end{bmatrix} + \begin{bmatrix} \mathbf{0} & \mathbf{0} & \mathbf{0} \\ \mathbf{0} & \mathbf{R} & \mathbf{0} \\ \mathbf{0} & \mathbf{0} & \mathbf{0} \end{bmatrix} \begin{bmatrix} \dot{\mathbf{U}} \\ \dot{\mathbf{Q}} \\ \dot{\mathbf{P}} \end{bmatrix} + \begin{bmatrix} \mathbf{K}_u + \mathbf{C}_{uV}\mathbf{K}_V^{-1}\mathbf{C}_{uV}^T & \mathbf{C}_{uV}\mathbf{K}_V^{-1} & -\mathbf{C}_{up} \\ \mathbf{K}_V^{-1}\mathbf{C}_{uV}^T & \mathbf{K}_V^{-1} & \mathbf{0} \\ \mathbf{0} & \mathbf{0} & \mathbf{K}_p \end{bmatrix} \begin{bmatrix} \mathbf{U} \\ \mathbf{Q} \\ \mathbf{P} \end{bmatrix} = \begin{bmatrix} \mathbf{F} \\ \mathbf{0} \\ \mathbf{0} \end{bmatrix} \tag{8}$$

where $\mathbf{Q} = (Q^{(1)}\, Q^{(2)} \cdots Q^{(P)})^T$ and $\mathbf{V} = (V^{(1)}\, V^{(2)} \cdots V^{(P)})^T$ are the column vectors of electric charges and potential differences; $\mathbf{R} = \text{diag}\,(R^{(1)}\, R^{(2)} \cdots R^{(P)})$ and $\mathbf{L} = \text{diag}\,(L^{(1)}\, L^{(2)} \cdots L^{(P)})$ are the diagonal matrices of the resistances and inductances of the patches; $\mathbf{U}$ and $\mathbf{P}$ are the vectors of nodal values of u_i and p; $\mathbf{M}_u$ and $\mathbf{K}_u$ are the mass and stiffness matrices of the structure (elastic structure and piezoelectric patches); $\mathbf{C}_{uV}$ is the electric mechanical coupled stiffness matrix; $\mathbf{K}_V = \text{diag}\,(C^{(1)}\, C^{(2)} \cdots C^{(P)})$ is a diagonal matrix filled with the P capacitances of the piezoelectric patches; $\mathbf{M}_p$ and $\mathbf{K}_p$ are the mass and stiffness matrices of the fluid; $\mathbf{C}_{up}$ is the fluid–structure coupled matrix; $\mathbf{F}$ is the applied mechanical force vector.

3. FE implementation of the coupled problem

In this section, the coupled finite element formulation is applied to the vibration analysis of an elastic/piezoelectric laminated plate coupled with an acoustic fluid.

3.1. Finite element discretization of the composite plate

Consider a laminated composite plate having an arbitrary constant thickness h and made N orthotropic elastic or piezoelectric layers.

3.1.1. Strain–displacements relations

We consider that sections normal to middle plane of the plate remain plane during deformation and the stress in the normal direction is negligible ($\sigma_{zz} = 0$). With these two classical assumptions, the total state of deformation can be described by the displacements u_0, v_0 and w_0 of the middle surface ($z = 0$) and the rotations θ_x and θ_y about the y and x axes, respectively (see Fig. 2). Thus the local displacements in the directions of the x, y and z axes are given by

$$u = u_0(x,y) - z\theta_x(x,y) \tag{9a}$$
$$v = v_0(x,y) - z\theta_y(x,y) \tag{9b}$$
$$w = w_0(x,y) \tag{9c}$$

With these notations, the state of strain at any point x, y (on the plate) and z (distance from the neutral surface), is equal to the sum of the middle surface strain (membrane) and the strain due to the changes of curvature. Denoting the middle surface extensional strains in the x and y directions by ϵ_{xx} and ϵ_{yy}, the middle surface changes in curvature by κ_{xx} and κ_{yy}, and the middle surface in-plane shear and warping by ϵ_{xy} and κ_{xy}, the state of the in-plane strain can be written as

$$\varepsilon_{xx} = \epsilon_{xx} - z\kappa_{xx} \tag{10a}$$
$$\varepsilon_{yy} = \epsilon_{yy} - z\kappa_{yy} \tag{10b}$$
$$2\varepsilon_{xy} = \epsilon_{xy} - z\kappa_{xy} \tag{10c}$$

where the middle surface extensional strain and curvatures are defined by

$$\epsilon_{xx} = \frac{\partial u_0}{\partial x}, \quad \kappa_{xx} = \frac{\partial \theta_x}{\partial x} \tag{11}$$
$$\epsilon_{yy} = \frac{\partial v_0}{\partial y}, \quad \kappa_{yy} = \frac{\partial \theta_y}{\partial y} \tag{12}$$
$$\epsilon_{xy} = \frac{\partial u_0}{\partial y} + \frac{\partial v_0}{\partial x}, \quad \kappa_{xy} = \frac{\partial \theta_x}{\partial y} + \frac{\partial \theta_y}{\partial x} \tag{13}$$

For thin plates, the transverse shear components ($\gamma_{xz} = \frac{\partial w}{\partial x} - \theta_x$ and $\gamma_{yz} = \frac{\partial w}{\partial y} - \theta_y$) are neglected ($\gamma_{xz} = \gamma_{yz} = 0$) inducing these additional relations:

$$\theta_x = \frac{\partial w}{\partial x}, \quad \theta_y = \frac{\partial w}{\partial y} \tag{14}$$

The strain components can be rewritten in the following matrix form

$$\boldsymbol{\varepsilon} = \mathbf{D} \begin{bmatrix} u_0 \\ v_0 \\ w \\ \theta_x \\ \theta_y \end{bmatrix} \tag{15}$$

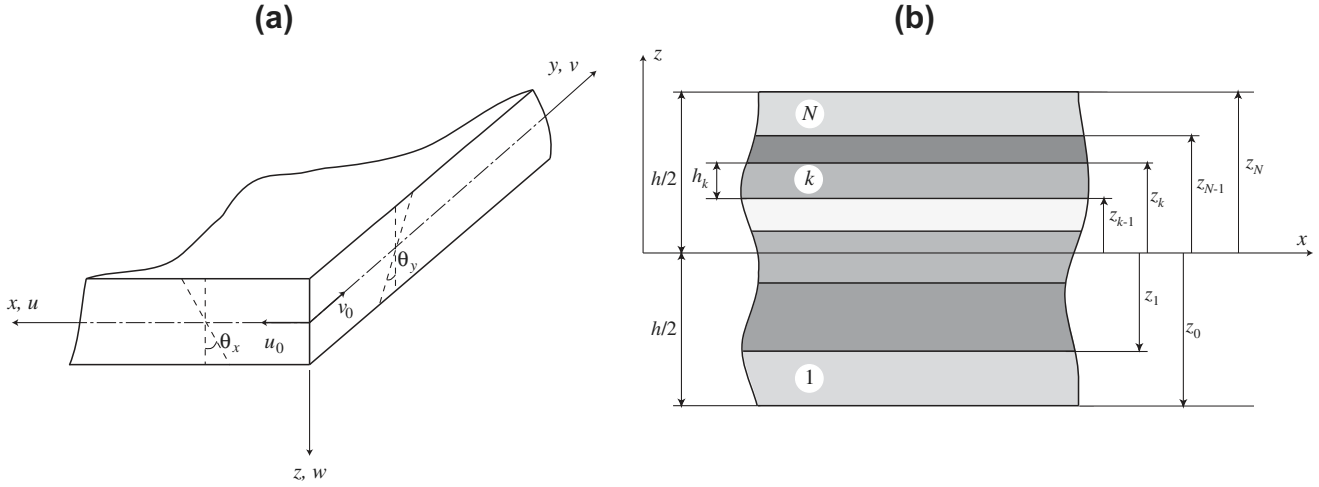

Fig. 2. Composite plate: (a) definitions of variables for plate approximations: displacements and rotations, and (b) cross section view of the layers.

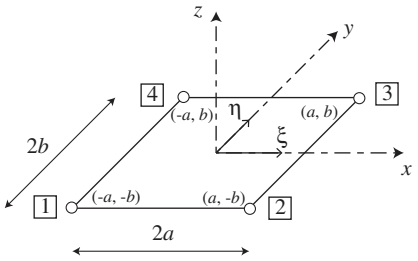

Fig. 3. A rectangular plate element.

with $\boldsymbol{\varepsilon} = [\,\epsilon_{xx} \quad \epsilon_{yy} \quad \epsilon_{xy} \quad \kappa_{xx} \quad \kappa_{yy} \quad \kappa_{xy}\,]^T$ and the gradient operator

$$\mathbf{D} = \begin{bmatrix} \frac{\partial}{\partial x} & 0 & 0 & 0 & 0 \\ 0 & \frac{\partial}{\partial y} & 0 & 0 & 0 \\ \frac{\partial}{\partial y} & \frac{\partial}{\partial x} & 0 & 0 & 0 \\ 0 & 0 & 0 & \frac{\partial}{\partial x} & 0 \\ 0 & 0 & 0 & 0 & \frac{\partial}{\partial y} \\ 0 & 0 & 0 & \frac{\partial}{\partial y} & \frac{\partial}{\partial x} \end{bmatrix} \tag{16}$$

3.1.2. Degrees-of-freedom and shape functions

Consider a rectangular element of a plate coinciding with the *xy* plane as shown in Fig. 3. Each node n (n = 1,2,3,4) has five degrees-of-freedom to describe the middle surface displacements u_{0n}, v_{0n} and w_n along the x, y and z directions, the rotation θ_{xn} about the y axis, and the rotation θ_{yn} about the x axis.

The elementary degrees-of-freedom vector $\mathbf{U}^e$, of size (20×1), is then defined in terms of the nodal dof vector $\mathbf{U}_n$ by

$$\mathbf{U}^e = \begin{bmatrix} \mathbf{U}_1 \\ \mathbf{U}_2 \\ \mathbf{U}_3 \\ \mathbf{U}_4 \end{bmatrix}, \quad \text{with} \quad \mathbf{U}_n = \begin{bmatrix} u_{0n} \\ v_{0n} \\ w_n \\ \theta_{xn} \\ \theta_{yn} \end{bmatrix}, \quad n = 1,2,3,4 \tag{17}$$

The displacements u_0 and v_0 are assumed to vary linearly along the axial co-ordinates x and y and they are discretized by Lagrange bi-linear shape functions, while the transverse displacement w and the rotations θ_x and θ_y are discretized by nonconforming cubic Hermite polynomial [21]. Thus, the elementary middle surface displacements and rotations of the plate are given in terms of the elementary degrees-of-freedom vector by

$$\begin{bmatrix} u_0^e \\ v_0^e \\ w^e \\ \theta_x^e \\ \theta_y^e \end{bmatrix} = \mathbf{N}(x,y)\mathbf{U}^e \tag{18}$$

where the interpolation matrix is defined by

$$\mathbf{N} = [\,\mathbf{N}_1 \quad \mathbf{N}_2 \quad \mathbf{N}_3 \quad \mathbf{N}_4\,] \tag{19}$$

and

$$\mathbf{N}_n = \begin{bmatrix} N_n^{\ell} & 0 & 0 & 0 & 0 \\ 0 & N_n^{\ell} & 0 & 0 & 0 \\ 0 & 0 & N_n^{c1} & N_n^{c2} & N_n^{c3} \\ 0 & 0 & \frac{\partial N_n^{c1}}{\partial x} & \frac{\partial N_n^{c2}}{\partial x} & \frac{\partial N_n^{c3}}{\partial x} \\ 0 & 0 & \frac{\partial N_n^{c1}}{\partial y} & \frac{\partial N_n^{c2}}{\partial y} & \frac{\partial N_n^{c3}}{\partial y} \end{bmatrix}, \quad n = 1,2,3,4 \tag{20}$$

with the linear N_n^{ℓ} and cubic N_n^{c1}, N_n^{c2} and N_n^{c3} $(n = 1, 2, 3, 4)$ shape functions given in the reference element [29]

$$N_n^{\ell} = \frac{1}{4}\xi_n\eta_n(\xi + \xi_n)(\eta + \eta_n) \tag{21a}$$

$$N_n^{c1} = \frac{1}{8}(1 + \xi\xi_n)(1 + \eta\eta_n)(2 + \xi\xi_n + \eta\eta_n - \xi^2 - \eta^2) \tag{21b}$$

$$N_n^{c2} = \frac{1}{8}\xi_n(\xi\xi_n - 1)(1 + \eta\eta_n)(1 + \xi\xi_n)^2 \tag{21c}$$

$$N_n^{c3} = \frac{1}{8}\eta_n(\eta\eta_n - 1)(1 + \xi\xi_n)(1 + \eta\eta_n)^2 \tag{21d}$$

in which $\xi = \frac{x}{a}$ and $\eta = \frac{y}{b}$ are the elementary co-ordinates that varies from -1 (when $x = -a$ for ξ and $y = -b$ for η) to 1 (when $x = a$ for ξ and $y = b$ for η), and where $\xi_n = \frac{x_n}{a}$ and $\eta_n = \frac{y_n}{b}$ (x_n and y_n corresponding to the co-ordinates of node n along the x and y directions as shown in Fig. 3).

Moreover, the elementary strain vector $\boldsymbol{\varepsilon}^e$ can be expressed by

$$\boldsymbol{\varepsilon}^e = \mathbf{B}\mathbf{U}^e \tag{22}$$

with the following discretized gradient operator

$$\mathbf{B} = \mathbf{D}\mathbf{N} \tag{23}$$

3.1.3. Elementary mass and stiffness matrices

The interpolations of displacements and strains presented in the previous section are used to express the elementary mass and stiffness matrices of the composite laminated plate.

The mass matrix is evaluated without neglecting rotational inertia. Using its definition given in the variational formulation ($\int_{\Omega_S} \rho_S \frac{\partial^2 u_i}{\partial t^2}\ \delta u_i\ \mathrm{d}v$), and combining Eqs. (9) and (18), the elementary mass matrix is defined by

$$\mathbf{M}_u^e = \int_{-1}^{1}\int_{-1}^{1} \mathbf{N}^T\mathbf{I}\mathbf{N}J_s(\xi,\eta)\ \mathrm{d}\xi\mathrm{d}\eta \tag{24}$$

where J_S is the Jacobien determinant of the transformation and $\mathbf{I}$ is the composite inertia matrix given by

$$\mathbf{I} = \begin{bmatrix} I_0 & 0 & 0 & -I_1 & 0 \\ 0 & I_0 & 0 & 0 & -I_1 \\ 0 & 0 & I_0 & 0 & 0 \\ -I_1 & 0 & 0 & I_2 & 0 \\ 0 & -I_1 & 0 & 0 & I_2 \end{bmatrix} \tag{25}$$

in which the zero I_0, first I_1 and second I_2 mass moments of inertia are given by

$$I_0 = \sum_{k=1}^{N} \rho_S^k(z_k - z_{k-1}), \quad I_1 = \frac{1}{2}\sum_{k=1}^{N} \rho_S^k(z_k^2 - z_{k-1}^2),$$

$$I_2 = \frac{1}{3}\sum_{k=1}^{N} \rho_S^k(z_k^3 - z_{k-1}^3)$$

In the same way, using its definition ($\int_{\Omega_S} c_{ijkl}\varepsilon_{kl}\delta\varepsilon_{ij}\ \mathrm{d}v$) and combining Eqs. (18) and (22), the elementary elastic stiffness matrix is given by

$$\mathbf{K}_u^e = \int_{-1}^{1}\int_{-1}^{1} \mathbf{B}^T\mathbf{C}\mathbf{B}J_s(\xi,\eta)\ \mathrm{d}\xi\mathrm{d}\eta$$

where $\mathbf{C}$ is the elasticity matrix of the composite given by

$$\mathbf{C} = \begin{bmatrix} A_{11} & A_{12} & A_{16} & B_{11} & B_{12} & B_{16} \\ A_{12} & A_{22} & A_{26} & B_{12} & B_{22} & B_{26} \\ A_{16} & A_{26} & A_{66} & B_{16} & B_{26} & B_{66} \\ B_{11} & B_{12} & B_{16} & D_{11} & D_{12} & D_{16} \\ B_{12} & B_{22} & B_{26} & D_{12} & D_{22} & D_{26} \\ B_{16} & B_{26} & B_{66} & D_{16} & D_{26} & D_{66} \end{bmatrix} \tag{26}$$

in which the extensional A_{ij}, bending D_{ij}, and extensional-bending B_{ij} coupling stiffness of the laminated composite are given by (see, e.g. [23])

$$A_{ij} = \sum_{k=1}^{N} \overline{Q}_{ij}^{k}(z_k - z_{k-1}), \quad B_{ij} = \frac{1}{2}\sum_{k=1}^{N} \overline{Q}_{ij}^{k}(z_k^2 - z_{k-1}^2),$$
$$D_{ij} = \frac{1}{3}\sum_{k=1}^{N} \overline{Q}_{ij}^{k}(z_k^3 - z_{k-1}^3)$$

where $i, j = 1,2,6$ and $\overline{Q}_{ij}^{k}$ represent the reduced material stiffness constants for each layer k in the global coordinate system deduced from the assumption of zero normal stress in the thickness direction.

3.2. Finite element discretization of the fluid domain

The aim of this section is to introduce the finite element discretization of the fluid domain. The considered domain is discretized with hexahedral elements. Each element is bounded by eight nodes and the nodal pressure is considered as the only nodal unknown variable.

The elementary pressure $p^e(x,y,z)$ can be expressed in terms of the vector of nodal pressures $\mathbf{P}^e$:

$$p^e(x,y,z) = \mathbf{N}_p(x,y,z)\mathbf{P}^e \tag{27}$$

where the interpolation matrix is defined by

$$\mathbf{N}_p = [N_1 \quad N_2 \quad N_3 \quad N_4 \quad N_5 \quad N_6 \quad N_7 \quad N_8]$$

with the following linear shape functions, given in the reference element:

$$N_n = \frac{1}{8}\xi_n\eta_n\zeta_n(\xi+\xi_n)(\eta+\eta_n)(\zeta+\zeta_n), \quad n = 1,\ldots,8$$

in which ξ, η and ζ are the elementary co-ordinates that varies from -1 to 1, and ξ_n, η_n and ζ_n correspond to the co-ordinates of the node n along the direction ξ, η and ζ, respectively, as shown in Fig. 4.

From its definition $\left(\frac{1}{\rho_F c_F^2}\int_{\Omega_F}\frac{\partial^2 p}{\partial t^2}\,\delta p\,\mathrm{d}v\right)$ given in the variational formulation, and using Eq. (27), the elementary mass matrix of the fluid can be expressed by

$$\mathbf{M}_p^e = \frac{1}{\rho_F c_F^2}\int_{-1}^{1}\int_{-1}^{1}\int_{-1}^{1}\mathbf{N}_p^T\,\mathbf{N}_p J_F\,\mathrm{d}\xi\,\mathrm{d}\eta\,\mathrm{d}\zeta \tag{28}$$

where J_F is the Jacobian determinant of the transformation from the real to the reference element.

In order to compute the elementary stiffness matrix of the fluid, we have to evaluate the pressure gradient using

$$\nabla p^e(x,y,z) = \mathbf{B}_p(x,y,z)\mathbf{P}^e \tag{29}$$

with the following discretized gradient operators

$$\mathbf{B}_p(x,y,z) = \left[\frac{\partial}{\partial x} \quad \frac{\partial}{\partial y} \quad \frac{\partial}{\partial z}\right]^T \mathbf{N}_p(x,y,z) \tag{30}$$

From definition $\left(\frac{1}{\rho_F}\int_{\Omega_F} p_{,i}\,\delta p_{,i}\,\mathrm{d}v\right)$, combining Eqs. (29) and (30), and transforming the discretized gradient operator in the reference coordinate system, the elementary stiffness matrix of the fluid can be expressed by

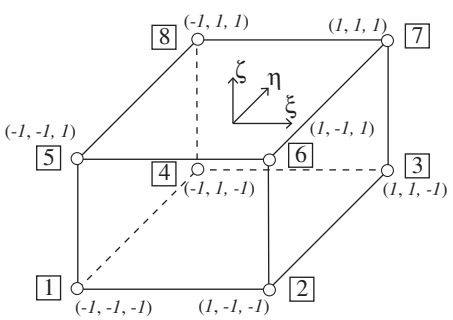

Fig. 4. Fluid hexahedric element.

$$\mathbf{K}_p^e = \frac{1}{\rho_F}\int_{-1}^{1}\int_{-1}^{1}\int_{-1}^{1}\mathbf{B}_p^T\mathbf{B}_p J_F\,\mathrm{d}\xi\,\mathrm{d}\eta\,\mathrm{d}\zeta \tag{31}$$

3.3. Elementary fluid–structure coupling matrix

Using the appropriate interface conditions at the common boundary between the fluid and the structure, the coupled fluid–structure matrix is derived. In first approach, a compatible mesh is considered at the interface so that the interface element can be easily defined. The interface element is bounded by four nodes, each having two degrees-of-freedom to describe the normal structure displacement w^e and the fluid pressure p^e.

The elementary normal displacement w^e is discretized by cubic shape functions and can be written, in terms of the nodal structure degrees-of-freedom, by

$$w^e = [\mathbf{N}_{w1} \quad \mathbf{N}_{w2} \quad \mathbf{N}_{w3} \quad \mathbf{N}_{w4}]\mathbf{U}^e = \mathbf{N}_w\mathbf{U}^e \tag{32}$$

where

$$\mathbf{N}_{wn} = \begin{bmatrix}0 & 0 & N_n^{c1} & N_n^{c2} & N_n^{c3}\end{bmatrix}, \quad n = 1,2,3,4 \tag{33}$$

The elementary pressure p^e is discretized by linear shape functions and can be written, in terms of nodal fluid pressure located at the interface, by

$$p^e = \begin{bmatrix}N_1^{\ell} & N_2^{\ell} & N_3^{\ell} & N_4^{\ell}\end{bmatrix}\begin{bmatrix}p_1\\p_2\\p_3\\p_4\end{bmatrix} = \mathbf{N}_{pi}\begin{bmatrix}p_1\\p_2\\p_3\\p_4\end{bmatrix} \tag{34}$$

Thus, the elementary coupling matrix of size (20×4), defined from the term $\int_\Sigma p\,n_i^F\,\delta u_i\,\mathrm{d}s$ in the variational formulation, can be written as

$$\mathbf{C}_{up}^e = \int_{-1}^{1}\int_{-1}^{1}\mathbf{N}_w^T\mathbf{N}_{pi}J_S\mathrm{d}\xi\,\mathrm{d}\eta \tag{35}$$

3.4. Extension to piezoelectric plate

In this section, we present an extension of the laminated composite plate to the case of piezoelectric layers with transverse polarization. The chosen multilayer model combines an equivalent single layer assumption for the mechanical displacement and a layerwise representation of the transverse electric potential (the electric potential is assumed to vary linearly in the thickness of each piezoelectric layer). The advantages of this mixed laminate theory are linked to its effectiveness to model thin composite plates and to capture the through-thickness electric heterogeneity induced by the piezoelectric layers.

From the previous electric potential assumption and neglecting the in-plane components, the electric field is defined, for each piezoelectric layer k, by its transverse component $E^k = -V^k/h_k$. V^k is the electrical potential difference between top and bottom surfaces and h_k is the layer thickness ($h_k = z_k - z_{k-1}$). We use in the finite element discretization only one degree of freedom to represent the electric potential differences V^k constant in each layer. Thus, the degrees-of-freedom of the plate element described in the previous section are augmented by the electric potential difference (voltage) of each layer.

The electric field of one multilayer piezoelectric plate element can be written in the following form:

$$\mathbf{E}^e = -\mathbf{B}_V\boldsymbol{V}^e \tag{36}$$

with $\mathbf{E}^e = [E^1 \cdots E^k \cdots E^N]^T$, $\boldsymbol{V}^e = [V^1 \cdots V^k \cdots V^N]^T$, and $\mathbf{B}_V = \mathrm{diag}\left(\frac{1}{h_1}\cdots\frac{1}{h_k}\cdots\frac{1}{h_N}\right)$.

With these considerations, the elementary electromechanical coupling stiffness matrix, given by $\sum_{n=1}^{N} \frac{V^{(n)}}{h^{(n)}} \int_{\Omega^{(p)}} e_{kij} n_k \delta\varepsilon_{ij} \, \mathrm{d}v$ in the variational formulation, can be written by

$$\mathbf{C}_{uV}^{e} = \int_{-1}^{1} \int_{-1}^{1} \mathbf{B}^{T} \mathbf{E} \mathbf{B}_{V} J_s(\xi, \eta) \, \mathrm{d}\xi \mathrm{d}\eta \tag{37}$$

E being the membrane-electric and bending-electric coupling matrix, defined by

$$\mathbf{E} = \begin{bmatrix} h_1 \bar{e}_{31}^{1} & \cdots & h_k \bar{e}_{31}^{k} & \cdots & h_N \bar{e}_{31}^{N} \\ h_1 \bar{e}_{32}^{1} & \cdots & h_k \bar{e}_{32}^{k} & \cdots & h_N \bar{e}_{32}^{N} \\ h_1 \bar{e}_{36}^{1} & \cdots & h_k \bar{e}_{36}^{k} & \cdots & h_N \bar{e}_{36}^{N} \\ \frac{z_1^2 - z_0^2}{2} \bar{e}_{31}^{1} & \cdots & \frac{z_k^2 - z_{k-1}^2}{2} \bar{e}_{31}^{k} & \cdots & \frac{z_N^2 - z_{N-1}^2}{2} \bar{e}_{31}^{N} \\ \frac{z_1^2 - z_0^2}{2} \bar{e}_{32}^{1} & \cdots & \frac{z_k^2 - z_{k-1}^2}{2} \bar{e}_{32}^{k} & \cdots & \frac{z_N^2 - z_{N-1}^2}{2} \bar{e}_{32}^{N} \\ \frac{z_1^2 - z_0^2}{2} \bar{e}_{36}^{1} & \cdots & \frac{z_k^2 - z_{k-1}^2}{2} \bar{e}_{36}^{k} & \cdots & \frac{z_N^2 - z_{N-1}^2}{2} \bar{e}_{36}^{N} \end{bmatrix} \tag{38}$$

where $\bar{e}_{3j}^{k} (j = 1, 2, 6)$ are the reduced piezoelectric constants for each layer k in the global coordinate system deduced from the assumption of zero normal stress in the thickness direction.

Finally, from $\sum_{n=1}^{N} \delta V^{(n)} C^{(n)} V^{(n)}$, the electric matrix is given by $\mathbf{K}_V = \mathrm{diag}\ (C^1 \cdots C^k \cdots C^N)$ where $C^k = \bar{\epsilon}_{33} S^k / h_k$ is the capacitance of the piezoelectric layer k ($\bar{\epsilon}_{33}^{k}$ is the dielectric permittivity in the thickness direction and S^k being the area of the layer).

4. Numerical examples

4.1. Free vibrations of a simply supported plate with surface-bonded piezoelectric layers

In order to validate the proposed composite piezoelectric plate finite element, we consider in this first example the free vibration problem of a five layers simply supported square laminated plate with surface-bonded piezoelectric layers. The geometrical data are given in Fig. 5 (length $a = 1m$ and total thickness $h = a/50 = 20$ mm). The layered configuration consists of three layers cross ply [0/90/0] graphite-epoxy and 2 layers of PZT-4. The thickness of each ply is indicated in Fig. 5. The material data are given in Table A.4 and the densities are considered to be unitary (1 kg m^{-3}) to allow comparisons with other available results. The assumed boundary conditions are $v = w = 0$ on the edges $x = 0$, a and $u = w = 0$ on the edges $y = 0$, a.

The first five fundamental frequency parameters, $\lambda = fa^2 \sqrt{\rho}/h \times 10^3$ in Hz (kg/m)$^{1/2}$ are calculated with the present finite element model and compared in Table 1 to: (i) a Higher Shear Deformation Theory using quadrilateral finite element with nine nodes and 11° of freedom by node (Q9-HSDT 11P) [4], (ii) a Third Order Shear Deformation Theory using quadrilateral finite element with four nodes and 7 degrees of freedom by node (TDST) [11], and (iii) an exact two-dimensionnal solution based on layerwise first-order shear deformation theory and quadratic non-uniform electric potential [1]. Two sets of electric boundary conditions are considered: short-circuited (SC) and open-circuited (OC).

The results obtained with the present element, with only 4 nodes and 5 dofs per node, are in good agreement with the other solutions in particular with the more refined element Q9-HSDT 11P. As the solution with TSDT element, differences between eigenfrequencies for piezoelectric layers in SC and OC conditions occur only in symmetric modes, which seems reasonable since asymmetric modes leads to asymmetric distribution of electric potential on the electrodes of piezoelectric layers leading to a charge cancelation effect [11]. For the first and fifth modes, as expected, the natural frequencies are higher in the open-circuited case than in the closed-circuited one. This weak difference should not be neglected and might be used to assess the piezoelectric effect through the so-called effective modal electromechanical coupling coefficient [28].

4.2. Vibration reduction of a cantilevered beam using a resonant shunt circuit

We consider in this second example a cantilever beam partially covered with two collocated piezoelectric elements, polarized in opposite directions (Fig. 6). The electrodes are connected in series to a passive electrical circuit composed of a resistor R and an inductor L, thus constituting a resonant shunt. The beam material is in aluminum with Young's modulus $E_b = 74$ GPa, Poisson's ratio $\nu_b = 0.34$ and density $\rho_b = 2800$ kg m^{-3}. For the piezoelectric patches, the following isotropic mechanical properties are used: Young's modulus $E_p = 57$ GPa, Poisson's ratio $\nu_p = 0$ and density $\rho_p = 7800$ kg m^{-3}. These parameters are chosen in order to simplify the comparison between the proposed plate model and the beam model developed in [28]. FInally, the piezoelectric constants are $e_{31} = e_{32} = 13.222$ C m^{-2} and $e_{36} = 0$, and the electrical permittivity (in the polarization direction) is $\epsilon_{33}/\epsilon_0 = 2400$. The geometrical data of the problem are given in Fig. 6.

Table 2 presents the first flexural natural frequencies of the cantilever structure in short-circuit and open-circuit conditions. The results obtained with the developed plate element are compared with those computed with a laminated piezoelectric finite element beam developed in [28]. This element has three mechanical degrees of freedom (axial displacement u, transverse displacement w and fiber rotation θ) and one electric degree of freedom per piezoelectric patch representing the uniform voltage in each patch. This beam model does not include any torsion which explains

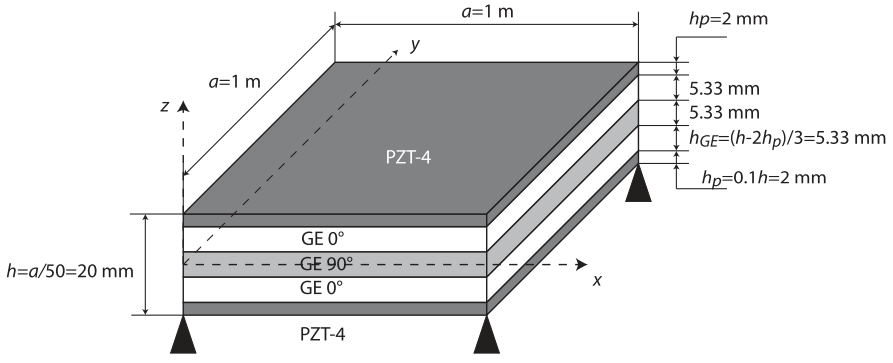

Fig. 5. Five layers simply supported square laminated plate: geometrical data.

Table 1
First five frequency parameters $\lambda = fa^2\sqrt{\rho}/h \times 10^3$ Hz $(\mathrm{kg/m})^{1/2}$.

Mode	Short circuited				Open circuited			
	Present	Q9-HSDT 11P	TSDT	Exact 2D	Present	Q9-HSDT 11	TSDT	Exact 2D
1	231.42	230.46	225.98	246.07	236.60	250.50	239.41	246.07
2	521.88	520.38	542.29	559.62	521.88	583.19	542.29	559.62
3	667.91	662.91	680.11	693.60	667.91	695.70	680.11	693.61
4	909.34	908.46	906.09	967.14	909.34	980.36	906.09	967.48
5	1027.22	1022.09	1099.05	1091.46	1030.47	1145.41	1100.94	1091.48

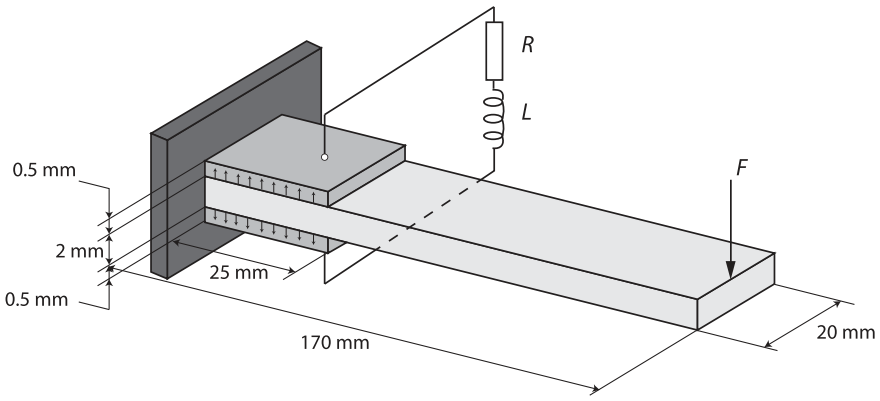

Fig. 6. Cantilever beam partially covered with two collocated piezoelectric elements: geometrical data.

the absence of these modes in Table 2. For the first five flexural modes, a very good agreement between the two models is obtained for the two electric boundary conditions. As in the previous example, the natural frequencies are slightly higher in the open circuited case than in the short circuited case due to the electromechanical coupling.

The beam is now excited by a normal sinusoidal force applied at its tip. The vibration output is detected at the excitation point, where the displacement reaches a maximum. The frequency responses, in the short-circuited and shunted cases are plotted and compared in Fig. 7. In this example, the resonant shunt is tuned in order to achieve maximum energy dissipation of the second mode. The optimal values of the resistor and inductor, calculated through the formulas given in [13,3], are $R = 8000\ \Omega$ and $L = 15$ H.

Fig. 7 shows that the resonant magnitude of the second mode has been significantly reduced. In fact, the strain energy contained in the piezoelectric material is converted into electrical energy and hence dissipated into heat using the *RL* shunt device.

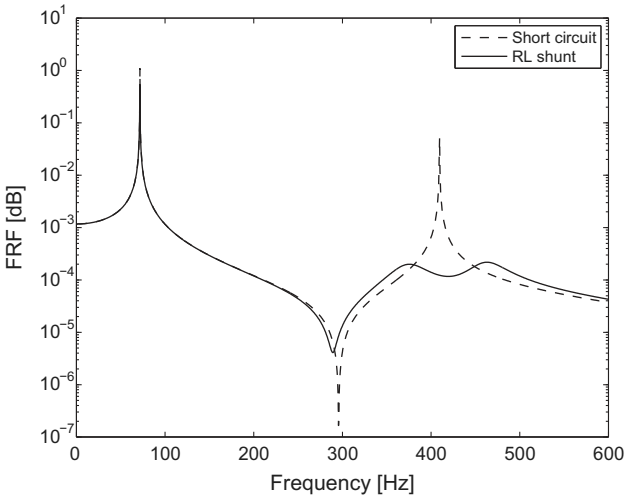

Fig. 7. Frequency response function: transverse displacement amplitude in dB at the excited point for short circuit and RL shunt damped configurations.

4.3. Vibration reduction of an elasto-acoustic coupled system

We present in this last example the analysis of an interior damped structural–acoustic systems using an inductive shunt damping technique, according to the finite element formulation described in this paper. First, the modal analysis of the electromechanical-acoustic problem is presented. Then, the frequency response of the coupled system in short-circuited and shunted cases are compared in terms of vibration amplitude and radiated sound power level.

We consider a 3D hexaedric acoustic cavity of size $A = 0.5$ m, $B = 0.3$ m and $C = 0.4$ m along the directions x, y, and z, respectively. The cavity is completely filled with air (density $\rho = 1.2\ \mathrm{kg/m^3}$ and speed of sound $c = 340$ m/s). The cavity walls are rigid except the top one, which is a flexible aluminum plate of thickness 1 mm clamped at its four edges. The density of the plate is $2700\ \mathrm{kg/m^3}$, the Young's modulus is 72 GPa and Poisson ratio 0.35. On the top surface of the plate, a PIC 151 patch is bonded, whose in plane dimensions are $0.1 \times 0.06\ \mathrm{m^2}$ along x and y and 0.5 mm thick (see Fig. 8). The mechanical characteristics of the piezoelectric material PIC 151 are given in Table A.4 in the Appendix A.

Table 2
Natural frequencies in Hz for short-circuit and open-circuit boundary conditions: comparison between plate and beam finite element formulations.

Mode	Short circuited		Open circuited	
	Present	Beam model	Present	Beam model
1 Flex. F1	69.0	69.0	69.8	69.8
2 Flex. F2	414.2	414.0	419.2	418.9
3 Flex. F3	1110.8	1108.0	1122.0	1119.3
4 Flex. F4	2081.7	2070.7	2093.6	2082.7
5 Flex. F5	3343.6	3312.5	3348.3	3317.4

Concerning the finite element discretization, we have used, for the structural part, 100 plate elements. The portion of the plate covered by the piezoelectric patch and the patch itself has been modeled according to the presented laminated theory. Moreover, only one electrical degree-of-freedom is used to represent the electrical charge Q in the patch. The acoustic cavity is discretized using $10 \times 10 \times 10$ hexahedric elements. The structural and acoustic meshes are compatible at the interface.

Table 3 presents the eigenfrequencies in three cases: (i) the 3D rigid acoustic cavity, (ii) the clamped plate with the patch in short- and open-circuited cases and (iii) the plate/acoustic-cavity coupled system in the short circuited case. Some results are compared with those given by the finite element code Nastran using the same mesh. The results presented in Table 3 show the excellent performance of our finite element model compared to Nastran and enables us to check the validity of the fluid–structure proposed formulation. The first nine coupled frequencies are associated with the first vibration modes of the structure lower than 345 Hz, and the last coupled frequency corresponds to the first acoustic mode in the rigid cavity. This can be confirmed by comparing the mode shapes in case (iii) with those obtained in case (i) or case (ii), which are not shown here for the sake of brevity. Moreover, as expected, the natural frequencies of the coupled modes (structure dominated) are lower than those for the structure in vacuum (except for the first mode) due to the added-mass effect of the fluid.

The plate is now excited by a normal mechanical force of intensity 1 N (see Fig. 8). In order to obtain maximum vibration attenuation of the second coupled mode, the patch is tuned to an *RL* shunt circuit. The optimal values of the electrical circuit are $R = 750\,\Omega$ and $L = 10.85$ H. The vibratory response is calculated with a modal reduction approach using the first 10 in vacuo structural modes and the first 10 acoustic modes of the fluid in rigid cavity [6].

The mean quadratic normal velocity of the plate $\langle V^2 \rangle$ and the radiated sound power in the closure Π are used as the indicators for this example:

$$\langle V^2 \rangle = \frac{\omega^2}{2AB} \mathbf{w}^* \overline{\mathbf{M}}_u \mathbf{w} \tag{39}$$

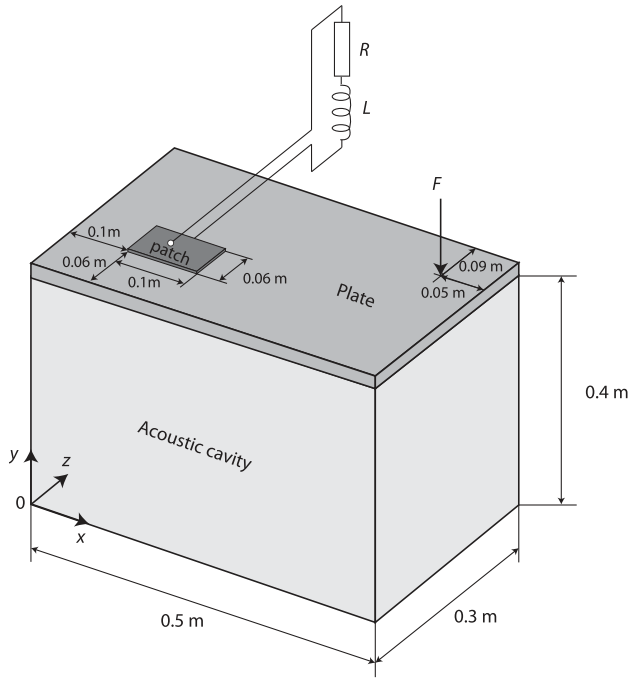

Fig. 8. Electromechanical-acoustic coupled system: geometrical data.

Table 3
Computed frequencies (Hz) of the structural–acoustic coupled system.

Fluid		Structure			Fluid–structure	
Nastan	Present	Nastran SC	Present SC	Present OC	Nastran	Present
341.40	341.40	70.04	70.40	70.43	78.46	76.23
426.75	426.75	99.94	100.45	100.80	98.76	99.30
546.51	546.51	156.18	156.71	156.93	155.94	156.04
569.00	569.00	180.32	180.56	180.56	178.97	179.07
663.56	663.56	204.17	204.55	204.69	203.15	203.21
691.23	691.23	234.56	232.96	233.24	233.36	231.40
711.25	711.25	249.01	251.93	252.10	248.17	250.62
788.94	788.94	317.31	318.66	319.02	316.76	317.44
812.35	812.35	343.82	334.91	336.69	341.25	333.55
864.04	864.04	347.19	346.86	346.99	342.71	341.49

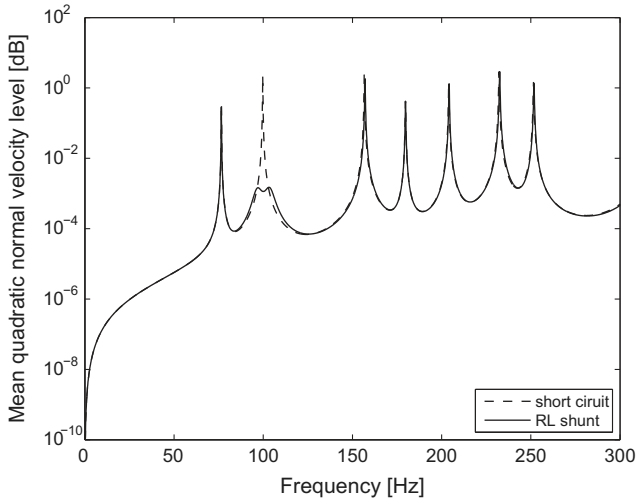

Fig. 9. The mean quadratic normal velocity of the plate with and without shunt system.

and

$$\Pi = \frac{1}{2} \mathrm{real}[\mathbf{w}^* \overline{\mathbf{C}}_{up} \mathbf{P}_w] \tag{40}$$

where ω is the angular frequency, $\mathbf{w}$ is the vector of nodal normal displacements of the plate, $\mathbf{P}_w$ is the vector of nodal pressures on the fluid–structure coupling surface. Note that $\overline{\mathbf{M}}_u$ and $\overline{\mathbf{C}}_{up}$ are the plate mass matrix and fluid–structure coupling matrix reduced to the dofs of interest.

The Figs. 9 and 10 present the mean quadratic normal velocity of the plate and the radiated sound power in the cavity with and without shunt. These figures show that resonant magnitude for the second mode has been significantly reduced due to the shunt damping effect.

5. Conclusion

This paper describes the variational formulation and the finite element implementation of vibroacoustic problems with piezoelectric shunt damping. The system under study consists of a multilayer piezoelectric structure (described by its displacement field and the electric potential differences of each piezoelectric layers) coupled with an acoustic fluid (described by its pressure field) and connected to resonant shunt circuits. The variational formulation of the fully coupled problem and the corresponding FE matrix equations are first presented. Then, an efficient finite element piezoelectric laminated plate and an appropriate fluid–structure interface element are developed. Finally, numerical examples are

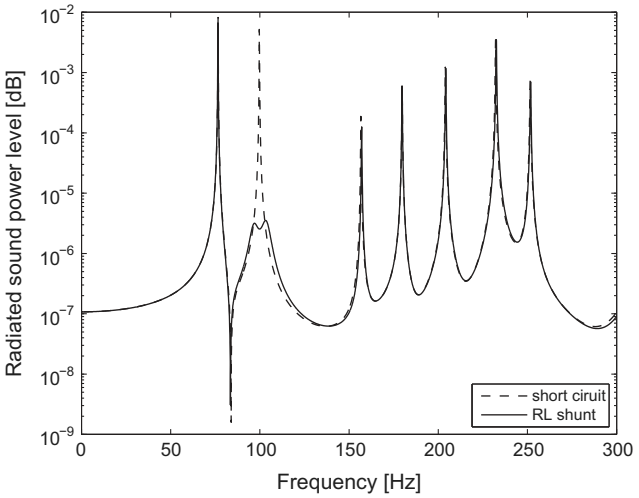

Fig. 10. The radiated sound power in the cavity with and without shunt system.

Table A.4
Properties of graphite-epoxy, PZT-4 and PIC151 materials (electric permittivity of air $\epsilon_0 = 8.85 \times 10^{-12}$ F m^{-1}).

Properties	Graphite-epoxy [26]	PZT-4 [1]	PIC 151 [20]
E_{11} (GPa)	132.38	81.3	66.71
E_{22} (GPa)	10.76	81.3	66.71
E_{33} (GPa)	10.76	64.5	48.81
G_{23} (GPa)	3.61	25.6	19.63
G_{13} (GPa)	5.65	25.6	19.63
G_{12} (GPa)	5.65	30.6	24.89
ν_{12} (GPa)	0.24	0.33	0.34
ν_{13} (GPa)	0.24	0.43	0.4223
ν_{23} (GPa)	0.24	0.43	0.4223
e_{15} (C m^{-2})	0	12.72	11.778
e_{24} (C m^{-2})	0	12.72	11.778
e_{31} (C m^{-2})	0	−5.2	−9.270
e_{32} (C m^{-2})	0	−5.2	−9.270
e_{33} (C m^{-2})	0	15.08	18.678
ϵ_{11}/ϵ_0	3.5	1475	1182
ϵ_{22}/ϵ_0	3	1475	1182
ϵ_{33}/ϵ_0	3	1300	905
ρ (kg m^{-3})	1578	7600	7800

presented in order to validate the FE implementations and to show the effectiveness of the proposed approach for the simulation of structural–acoustic vibration reduction problems by passive piezoelectric shunt damping techniques. In particular, the efficiency of the developed laminated piezoelectric plate element (relatively to the small number of degrees of freedom per node) has been highlighted and the passive inductive shunt damping techniques has been shown very effective for vibration attenuation of low frequency modes in structural–acoustics. To broaden the effectiveness of these inductive shunt systems on a wider frequency band and to avoid a very precise tuning of the electrical parameters, further investigations concern the extension of this work to switching shunt damping [12].

Appendix A

Table A.4.

References

[1] Benjeddou A, Deü J-F, Letombe S. Free vibrations of simply-supported piezoelectric adaptive plates: an exact sandwich formulation. Thin-Walled Struct 2002;40(7–8):573–93.
[2] Carrera E, Nali P. Multilayered plate elements for the analysis of multifield problems. Finite Elements Anal Des 2010;46(9):732–42.
[3] Corr L, Clark W. Comparison of low-frequency piezoelectric switching shunt techniques for structural damping. Smart Mater Struct 2002;11(3):370–6.
[4] Franco Correia VM, Aguiar Gomes MA, Suleman A, Mota Soares CM, Mota Soares CA. Modelling and design of adaptive composite structures. Comput Meth Appl Mech Eng 2000;185(2–4):325–46.
[5] Deü J-F, Larbi W, Ohayon R. Piezoelectric structural acoustic problems: symmetric variational formulations and finite element results. Comput Meth Appl Mech Eng 2008;197(19–20):1715–24.
[6] Deü J-F, Larbi W, Ohayon R. Structural–acoustic vibration reduction using piezoelectric shunt techniques: FE formulation and reduced order model. In: Proceedings of the 3rd international conference on computational methods in structural dynamics and earthquake engineering, COMPDYN2011. Corfu, Greece; 25–28 May 2011.
[7] Edery-Azulayand L, Abramovich H. Active damping of piezo-composite beams. Compos Struct 2006;74(4):458–66.
[8] Garcia Lage R, Mota Soares CM, Mota Soares CA, Reddy JN. Modelling of piezolaminated plates using layerwise mixed finite elements. Comput Struct 2004;82(23-26):1849–63.
[9] Gaudenzi P, Carbonaro R, Benzi E. Control of beam vibrations by means of piezoelectric devices: theory and experiments. Compos Struct 2000;50(4):373–9.
[10] Gopinathan SV, Varadan VV, Varadan VK. Finite element/boundary element simulation of interior noise control using active–passive control technique. Proc SPIE 2000;3984:22–32.
[11] Godoy TC, Trindade MA. Modeling and analysis of laminate composite plates with embedded active–passive piezoelectric networks. J Sound Vibr 2011;330(2):194–216.
[12] Guyomar D, Richard T, Richard C. Sound wave transmission reduction through a plate using a piezoelectric synchronized switch damping technique. J Intell Mater Syst Struct 2008;19(7):791–803.
[13] Hagood N, Von Flotow A. Damping of structural vibrations with piezoelectric materials and passive electrical network. J Sound Vibr 1991;146(2):243–68.
[14] Heidary F, Eslami MR. Piezo-control of forced vibrations of a thermoelastic composite plate. Compos Struct 2006;74(1):99–105.
[15] Kaljevic I, Saravanos DA. Steady-state response of acoustic cavities bounded by piezoelectric composite shell structures. J Sound Vibr 1997;204(3):459–79.
[16] Kim J, Ko B. Optimal design of a piezoelectric smart structure for noise control. Smart Mater Struct 1998;7(6):801–8.
[17] Larbi W, Deü J-F, Ohayon R. Vibration of axisymmetric composite piezoelectric shells coupled with internal fluid. Int J Numer Meth Eng 2007;71(12):1412–35.
[18] Larbi W, Deü J-F, Ciminello M, Ohayon R. Structural–acoustic vibration reduction using switched shunt piezoelectric patches: a finite element analysis. J Vibr Acoust 2010;132(5):051006 [9 pages].
[19] Lefèvre J, Gabbert U. Finite element simulation of smart lightweight structures for active vibration and interior acoustic control. Technische Mechanik 2003;23(1):59–69.
[20] Lin HY, Ma CC. The influence of electrode designs on the resonant vibrations for square piezoceramic plates. IEEE Trans Ultrason Ferroelect Freq Control 2006;53(5):825–37.
[21] Melosh RJ. Structural analysis of solids. J Struct Div: Proc Am Soc Civil Eng 1963:205–23.
[22] Morand HJ-P, Ohayon R. Fluid-structure interaction. New York: John Wiley & Sons; 1995.
[23] Reddy JN. Mechanics of laminated composite plates and shells: theory and analysis. Second ed. Boca Raton, FL: CRC Press; 2004.
[24] Ohayon R, Soize C. Structural acoustics and vibration. Mechanical models, variational formulations and discretization. Academic Press; 1998.
[25] Ro J, Baz A. Control of sound radiation from a plate into an acoustic cavity using active constrained layer damping. Smart Mater Struct 1999;8(3):292–300.
[26] Saravanos DA, Heyliger PR, Hopkins DA. Layerwise mechanics and finite element for the dynamic analysis of piezoelectric composite plates. Int J Solids Struct 1997;34(3):359–78.
[27] Shields W, Ro J, Baz A. Control of sound radiation from a plate into an acoustic cavity using active piezoelectric-damping composites. Smart Mater Struct 1998;7(1):1–11.
[28] Thomas O, Deü J-F, Ducarne J. Vibrations of an elastic structure with shunted piezoelectric patches: efficient finite element formulation and electromechanical coupling coefficients. Int J Numer Meth Eng 2009;80(2):235–68.
[29] Zienkiewicz OC, Taylor RL. The finite element method. The basis, vol. 1. Butterworth-Heinemann; 2001.